Int J CARS (2010) 5:29–37
DOI 10.1007/s11548-009-0379-x

ORIGINAL ARTICLE

Computer simulation of vertebral artery occlusion in endovascular procedures

Harvey Ho · Kumar Mithraratne · Holger Schmid · Gregory Sands · Peter Hunter

Received: 8 January 2009 / Accepted: 4 June 2009 / Published online: 23 June 2009

Abstract
Objective The aim of this work is to establish a computational pipeline for the simulation of blood flow in vasculatures and apply this pipeline to endovascular interventional scenarios, e.g. angioplasty in vertebral arteries.
Methods A patient-specific supra-aortal vasculature is digitized from a 3D CT angiography image. By coupling a reduced formulation of the governing Navier–Stokes equations with a wall constitutive equation we are able to solve the transient flow in elastic vessels. By further incorporating a bifurcation model the blood flow across vascular branches can be evaluated, thus flow in a large vasculature can be modeled. Vascular diseases are simulated by modifying the arterial tree configurations, e.g. the effective diameters, schematic connectivity, etc. Occlusion in an artery is simulated by removing that artery from the arterial tree.
Results It takes about 2 min per cardiac cycle to compute blood flow in an arterial tree consisting of 38 vessels and 18 bifurcations on a laptop PC. The simulation results show that blood supply in the posterior region is compensated from the contralateral vertebral artery and the anterior cerebral arteries if one of the vertebral arteries is occluded.
Conclusion The computational pipeline is computationally efficient and can capture main flow patterns at any point in the arterial tree. With further improvement it can serve as a powerful tool for the haemodynamic analysis in patient-specific vascular structures.

H. Ho (✉) · K. Mithraratne · G. Sands · P. Hunter
Bioengineering Institute, University of Auckland,
Auckland, New Zealand
e-mail: harvey.ho@auckland.ac.nz

H. Schmid
Department of Continuum Mechanics,
RWTH Aachen University, Aachen, Germany

Keywords Endovascular intervention · Vertebral artery · Blood flow · Model

Introduction

In 70% of the population, the two contralateral vertebral arteries arise from the subclavian arteries and merge into a single basilar artery which is the main pathway for posterior cerebral circulation (Fig. 1a) [1]. Severe atherosclerosis or occlusive lesions in the vertebrobasilar system may lead to infarction of brain tissues and cause ischemic stroke. The typical symptoms include unsteadiness of gait, bilateral sensory impairment, diplopia, etc. [1,2]. During the last two decades, endovascular intervention, i.e. angioplasty of the vertebral arteries has emerged as an effective method to treat severe vertebral lesions. In this procedure, a catheter is inserted into an artery from a puncture site (usually femoral artery) and advanced to the lesion site over a guidewire. A balloon installed at the end of the catheter is inflated to push open the lesion. A stent is then deployed to keep the lumen patent (Fig. 1b).

Since brain tissues are very sensitive to ischemia, the hemodynamic factors need to be carefully considered preoperatively to ensure optimal surgery. For example, how will a deployed endograft change flow patterns in the arterial tree or what possible complications may occur, etc. From this perspective computer simulations can play a positive role in assisting vascular surgeons' decision-making.

Numerous computer models of the cardiovascular system have been developed during the last several decades. These models range from lumped parameter (0D) models to 3D models, adapting to different scales of the cardiovascular system. 3D models are useful in capturing local flow patterns and effects, e.g. flow recirculation and wall shear stress (WSS)

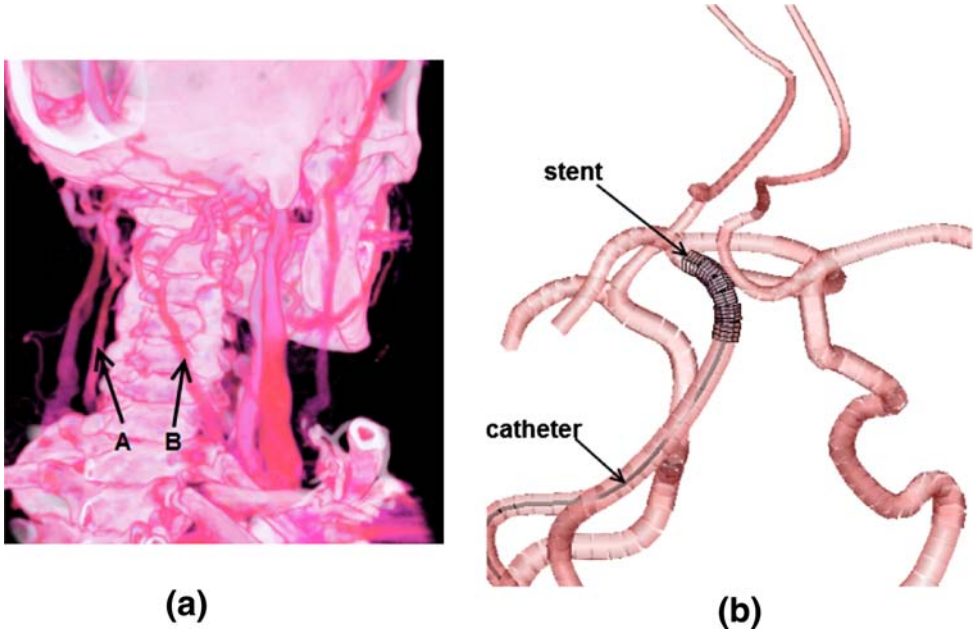

Fig. 1 **a** Visualization of a CT head image: the two *arrows* indicate two contralateral vertebral arteries. *A* and *B* are the two sites whose flow profiles are analyzed later in 'Endovascular intervention'; **b** Visualization of a catheter and a stent in angioplasty

in complex geometries like atherosclerotic arteries [3], bifurcations [4], and in tortuous arterial trees [5,6]. Since a large number of computational elements are usually required in 3D models, the computational cost can be infeasible for a large vasculature. A different strategy is to use a reduced version (1D) of the governing equations which considers the axial flow as the dominant flow. This approach has the advantage of substantially reduced computation cost and it has been used to model much larger vasculatures, e.g. the coronary arterial tree [7,8], the cerebral [9] and mesenteric vasculatures [10]. However, the 1D model is not capable of predicting complex flow patterns as in 3D models. It is also impractical to trace the huge number of small vessels at the arteriole and capillary levels where the blood cannot be modeled as a continuum. Instead, the lumped parameter approach is taken which ignores the actual geometries of these vessels and treats the circulation system as a 'black box' [11]. The overall hemodynamic behaviors, e.g. the vascular resistance and compliance can be modeled using the electronic analog (i.e. voltage for pressure, current for flow rate) [11]. This approach has been successfully used to model various systemic circulation phenomena such as the systemic load and compliance (e.g. Otto Frank's Windkessel model [12]), wave propagation in the arterial system [13], parametric analysis of vascular diseases [14], and also as the boundary treatment for 1D and 3D models [15,16]. However, since the axial variable (x) is not taken into the lumped parameter model equations they cannot model an arterial tree as per its geometrical details.

The vascular system we deal with in this work is a patient-specific cerebral arterial tree, which starts from the ascending aorta and ends at the efferent vessels of the circle of Willis. The 1D model is employed because of its benefit of substantially reduced computational cost compared with 3D models and its ability to evaluate flow at *any* point in the tree. In the sense of mathematical formation, our model is similar to that of [7–10] especially [9]. The difference between our model and that of [9], however, is that the arterial tree in our model was digitized from a *patient-specific* vasculature therefore the flow simulation can better reflect the actual vascular anatomy.

Methods

Vascular model construction

The 3D CT Angiography (CTA) image of Fig. 1a contains 421 slices with each slice 378 × 336 pixels in image matrix. The spatial resolution of the image is $0.488 \times 0.488 \times 0.7$ mm (Width × Height × Depth). Using an open source imaging and visualization tool CMGUI [17] we manually select 175 key points along the center line of large blood vessels as nodes. The radius at each node is defined as a field for that particular node. These nodes are then connected by one-dimensional (1D) cubic Hermite elements. Cylinders are constructed along these elements to represent the major arteries supplying blood to the brain. Figure 2 depicts this digitizing process.

The arterial tree shown in Fig. 2 consists of 38 arterial segments and 18 bifurcations. Vascular stenosis can be simulated by changing the *effective* diameter at the lesion sites, or by removing a vessel from the tree in case of complete occlusion.

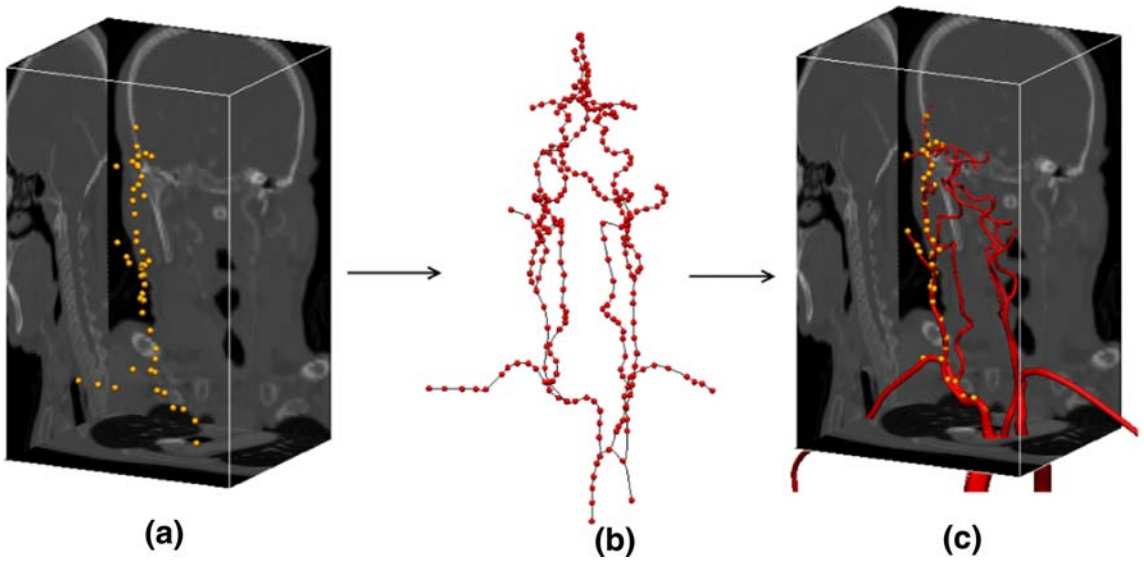

Fig. 2 Vascular tree construction pipeline: **a** Nodes selected manually; **b** 1D elements construction; **c** Cylinder simulation incorporating radius information

Hemodynamics modeling

Governing equations

In large arteries, the relative size of red cell to vessel diameter is small and blood can be modeled as an incompressible, homogeneous, Newtonian fluid [11,20]. We further assume that the flow in the circumferential direction is negligible and that the radial velocity is small compared to the axial velocity. The full 3D version of the governing equations can then be reduced to two 1D equations:

$$\frac{\partial R}{\partial t} + V\frac{\partial R}{\partial x} + \frac{R}{2}\frac{\partial V}{\partial x} = 0 \tag{1}$$

$$\frac{\partial V}{\partial t} + (2\alpha - 1)V\frac{\partial V}{\partial x} + 2(\alpha - 1)\frac{V^2}{R}\frac{\partial R}{\partial x} = -\frac{1}{\rho}\frac{\partial P}{\partial x} - 2\frac{\nu\alpha}{\alpha - 1}\frac{V}{R^2} \tag{2}$$

where V, R, P, ρ and ν represent velocity, inner vessel radius, transmural pressure, blood density and kinematic viscosity, respectively. The parameter α specifies axial velocity profile [18]:

$$V_r = \frac{\alpha}{2-\alpha}\bar{V}\left[1 - \left(\frac{r}{R}\right)^{\frac{2-\alpha}{\alpha-1}}\right] \tag{3}$$

where $\bar{V}$ represents the mean axial flow velocity. Different velocity profiles, including the parabolic profile ($\alpha = 1.3$) and the blunt profile ($\alpha = 1.1$), are shown in Fig. 3a.

To close the 1D system Eq. (1)–(2), an empirical wall constitutive equation [18] is introduced:

$$P(R) = Go\left[\left(\frac{R}{Ro}\right)^{\beta} - 1\right] \tag{4}$$

where Go is a stiffness reference, Ro the unstressed radius, β is the wall elasticity coefficient. Since the wall stiffness varies in the arterial tree, e.g. the intracranial arteries are stiffer that extracranial arteries, wall elasticity can be modeled by adjusting Go and β values in a combinative manner.

Boundary conditions

Pressure is selected as the inflow boundary condition (BC) because it is readily available in clinical environments. A physiologically realistic pulsatile pressure, which varies between 10.6 kPa (80 mmHg) and 16 kPa (120 mmHg) within 1 s (approximately one cardiac cycle) is shown in Fig. 3b.

The treatment of the outflow BC is more complicated because the resistance and compliance of the truncated downstream vessels need to be addressed properly. In this work, we use artificial elastic tubes, which we refer to as resistance segments (RSs) and attach them to the corresponding arterial tree outlets. The characteristics of a RS include its short length and rapidly tapering radii. Based on the mass conservation law, flow velocity increases rapidly when the blood flows through a RS. On the other hand, the blood pressure drops sharply due to Bernoulli effects. Hence, one of the main hemodynamic effects of resistance vessels, i.e. inducement of large pressure drop in the cardiovascular system, can be simulated via the RSs.

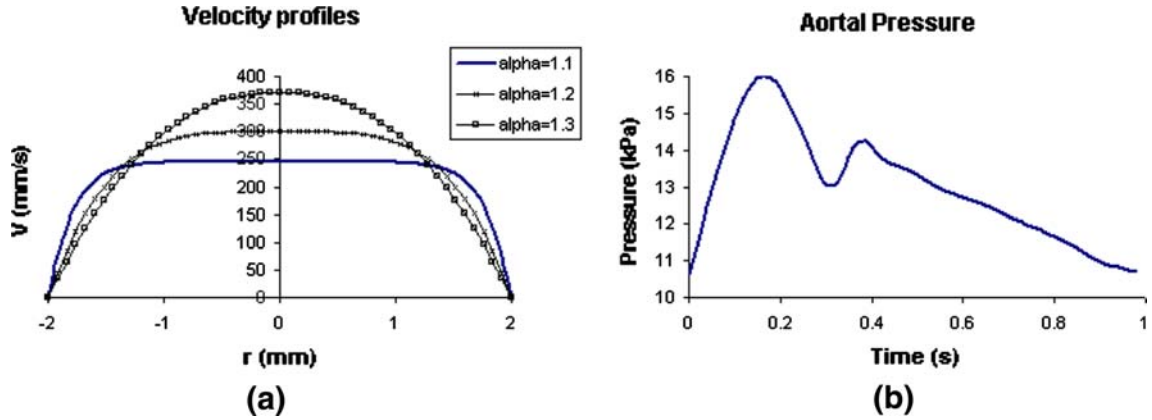

Fig. 3 **a** Different profiles corresponding to different α values; **b** Physiological pressure boundary condition

Numerical methods

The nonlinear, hyperbolic system (1–3) cannot be solved analytically. Numerical methods must be introduced to solve the equations. This requires the discretization of spatial and temporal domain into a finite number of grid elements. The number of grids is decided by the spatial step (Δx) and temporal step (Δt).

We adopt a predictor–corrector type MacCormack numerical scheme. In this scheme, the predicted values of P, R, V are evaluated by a backward difference, and their 'corrected' values are evaluated by a forward difference. The predictor–corrector procedure is applied for each time step. This scheme is second-order accurate in both space and time [19].

The stability analysis dictates that the numerical speed $\Delta x/\Delta t$ must be faster than the wave speed of the equation [7,10]. Since the propagation speed of the blood in an elastic tube is about 5–10 m/s [12], for a spatial step $\Delta x = 1$ mm, the time step Δt should be 0.1–0.2 ms.

Bifurcation model

To model flow in an arterial tree, a bifurcation model is further incorporated. Referring to Fig. 4, the vessel segments **a**, **b** and **c** represent the parent vessel and the two daughter vessels. If we assume that no fluid is stored at the junction point **o**, and zero energy is lost due to fluid viscosity, then by the law of mass conservation we have:

$$Fa - Fb - Fc = 0 \tag{5}$$

where F represents flow rate ($\pi R^2 V$). By manipulating Eq. (1) and (3) we have:

$$\frac{\partial P}{\partial t} + \frac{1}{2\pi R}\frac{\partial F}{\partial x}\frac{dP}{dR} = 0 \tag{6}$$

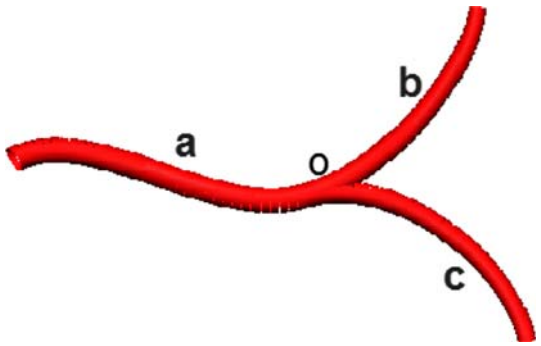

Fig. 4 Bifurcation model: **a** parent vessel; **b, c** daughter vessels; **o** junction

Applying the momentum conservation law for parent vessel **a** yields:

$$\pi R_a^2(P_a - P_o) = \frac{\partial(\rho l_a \pi R_a^2 V_a)}{\partial t} \tag{7}$$

where l_a are the radius and length of vessel **a**. Equations similar to Eq. (7) can be written for daughter vessels **b** and **c**. These equations are expanded using a central difference about each time step. The resulted equations, together with Eq. (5), are then solved by using a Newton–Raphson iterative scheme.

We refer the interested reader to literature [7,18] for more derivation and numerical scheme details of this bifurcation model.

Results

Normal arterial tree

Initial and boundary conditions

When solving the governing equations, the density ρ and viscosity ν of the blood are set as 1.05 g/cm^3 and 3.2 cm^2/s,

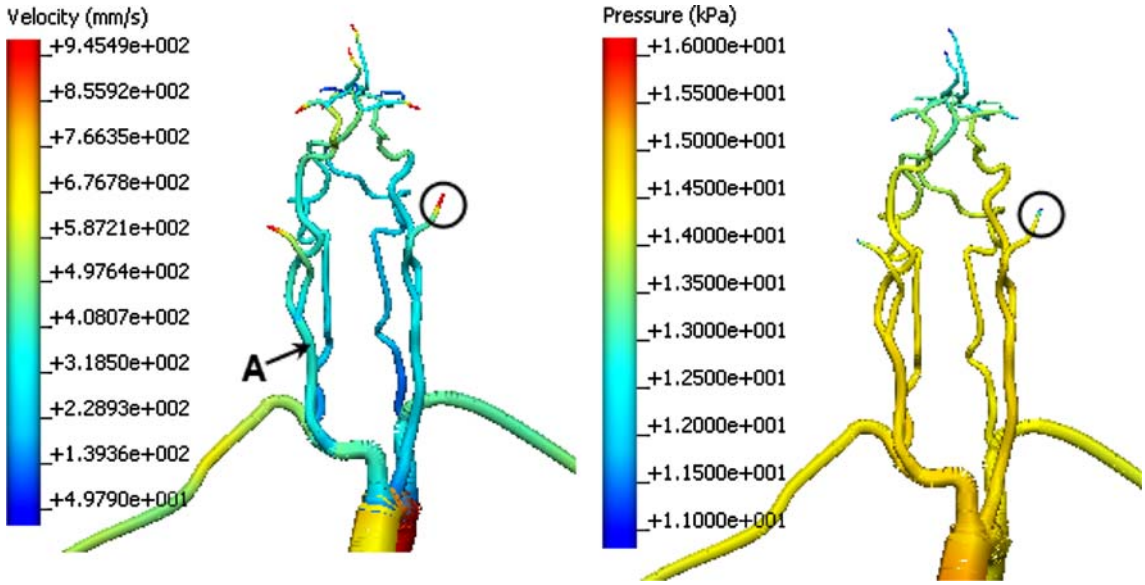

Fig. 5 Velocity and pressure distribution in the cerebral arterial tree at $t = 0.3$ s. The vessel segment inside the circle represents one of the resistance segments as the out boundary treatment: the velocity in this segment increases sharply whilst the pressure drops acutely due to Bernoulli effects; The velocity waveform at site *A* is recorded and compared with Doppler ultrasound measurement (refer to Fig. 6)

respectively. The initial velocity at all vessel segments is 0 mm/s. The initial pressure is 10.6 kPa (80 mmHg). The data of vessel wall elasticity is taken from [9], which are translated into their corresponding Go(10–15 kPa) and β (= 2) values. The spatial size Δx of the finite difference grid is set as 1 mm, which discretizes the arterial tree into 2,570 grids. The temporal step Δt is 0.1 ms. The number of total time steps in a cardiac cycle therefore is therefore 10,000.

Computational results

It takes about 12 min to compute the flow in five cardiac cycles on a personal computer (1.73 GHz, 3G RAM, Intel Pentium Dual-Core) and the flow data in the last cardiac cycle are analyzed. The computational results contain important hemodynamic data in the whole arterial tree, e.g. the pressure, velocity and flow rate. Figure 5 visualizes the pressure and velocity distribution in the arterial tree at $t = 0.3$ s.

Validation

The velocity waveform of site A in Fig. 5 is shown in the chart of Fig. 6. To validate this result, a LogicScan 128 ultrasound scanner (TELEMED Ltd., Lithuania) is used to detect the flow velocity at the same location (i.e. the right common carotid artery) from a healthy volunteer. The measured waveform is shown in the image of Fig. 6. A comparison between the two waveforms indicates that the largest velocity (about 31–32 cm/s, occurs at systole) of the simulation matches that of the ultrasound data. However, the simulation overestimates the flow velocity at diastole. On the other hand, the mean flow velocity (18.6 cm/s) of the CCA agrees with the data (e.g. 16.9 cm/s in Perktold et al. [4]) adopted in the 3D carotid studies. We assume the overall simulation result is within the acceptable physiological range of *in vivo* ultrasonic measurement.

We also compare the velocity waveform of vertebral artery with published ultrasound data by Buckenham and Wright [21], as shown in Fig. 7. The comparison indicates that the ultrasound measurement has a higher peak systole velocity and a lower diastole velocity than our model. However, the average velocities of the two waveforms (20.1 cm/s from our model, 22.6 cm/s from ultrasound) are consistent.

We further check if mass is conserved across the tree. In this study we take two bifurcation sites, the carotid artery (CA) and middle cerebral artery (MCA) as the examining points and record their flows at 0.05 s as tabulated in Table 1.

Table 1 shows that the difference between the flow in the parent vessel and the sum of two daughter vessels has an error of approximately 3% for transient flow. In steady flow the error rate is much lower (<0.1%).

Effects of vertebral occlusion

If we assume that one of the vertebral arteries is occluded by severe stenosis, or by an inflated balloon, e.g. at site B in Fig. 1a, the corresponding modification to the network topology is to remove VA2 (see Fig. 8) from the arterial tree because there is no flow in that artery. The BC are set as the same as normal flow, i.e. a pulsatile pressure waveform

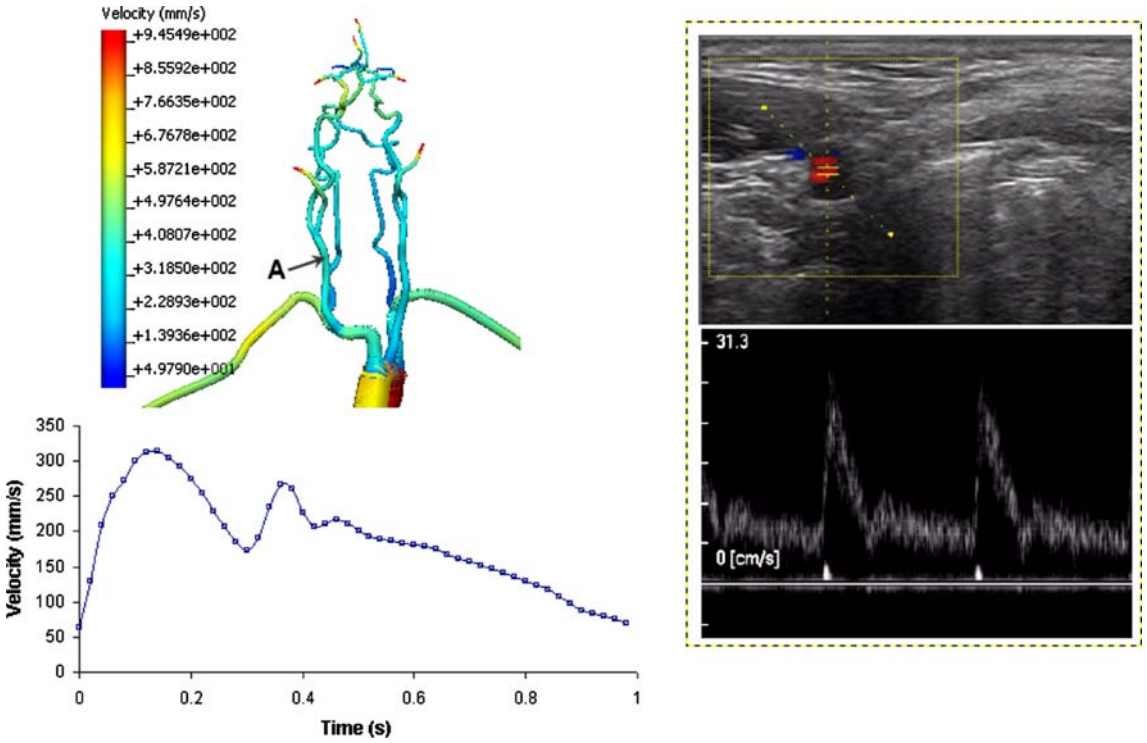

Fig. 6 Comparison of the velocity waveform in the common carotid artery (site *A* in the arterial tree): the largest magnitude of the velocity at systole (31–32 cm/s) from the simulation well matches that of the ultrasound data; the velocity in the diastole is overestimated, however the average velocity agrees with literature, e.g. as reported in [4]

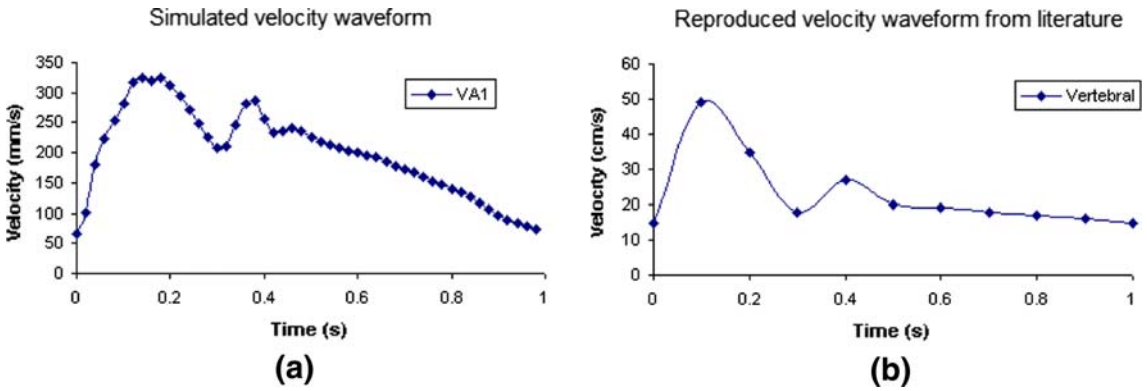

Fig. 7 Comparison of the velocity waveform in the vertebral artery: **a** the waveform from our simulation; **b** the waveform reproduced from ultrasound image as reported by Buckenham and Wright [21]

is prescribed from the inlet (ascending aorta), and a fixed pressure (10.6 kPa) is imposed from the outlets of the RSs, which are attached to the distal ends of the original arterial tree. We then record and observe the flow in VA1 from site A.

The visualizations of the velocity distribution (at $t = 0.5$ s) before and after vertebral occlusion are shown in Fig. 8a, b, respectively. Since there is no flow in VA2 (i.e. velocity is 0 mm/s), it appears in the dark blue color. A visual inspection of the right vertebral artery (VA1) and the left posterior communicating artery (L. PCoA) suggests that the flow velocities in them have increased after VA2 occlusion. We further check the velocity waveforms in these arteries, which are shown in Fig. 8c, d. The simulation suggests that the flow increase in VA1 is about 5–100 mm/s with an average of 52 mm/s. This increase, however, is not sufficient to

Table 1 Comparison of flow rate (unit: mm/s) at bifurcation sites

Vessels	CA	MCA
Daughter vessel 1	6.35	6.33
Daughter vessel 2	10.10	1.21
Sum	16.45	7.54
Parent vessel	16.88	7.83
Simulation error	0.43 (2.5%)	0.29 (3.7%)

The parent vessel, daughter vessels 1 and 2 refer to: (a) common, external and internal carotid artery in CA; (b) internal carotid artery, middle and anterior cerebral artery in MCA, respectively

compensate the lost blood supply due to VA2 occlusion. The waveform in L. PCoA, on the other hand, shows that the blood supply from the anterior cerebral arteries has increased (velocity increase by average 30 mm/s) when a complete CoW is present.

Discussion

Endovascular intervention is a fast evolving surgical discipline and is being researched in laboratories throughout the world's hospitals, universities and industry [22]. Clinicians continue to develop and apply novel techniques to provide safer, more effective therapies to patients. Applying these techniques to clinical environment requires a sound understanding of hemodynamics in the vascular systems. Computer simulation can play a positive role in planning operations, understanding pathologies and developing endo-devices, etc. [12].

In this work we employed a 1D system to model the blood flow in a patient-specific cerebral tree digitized from

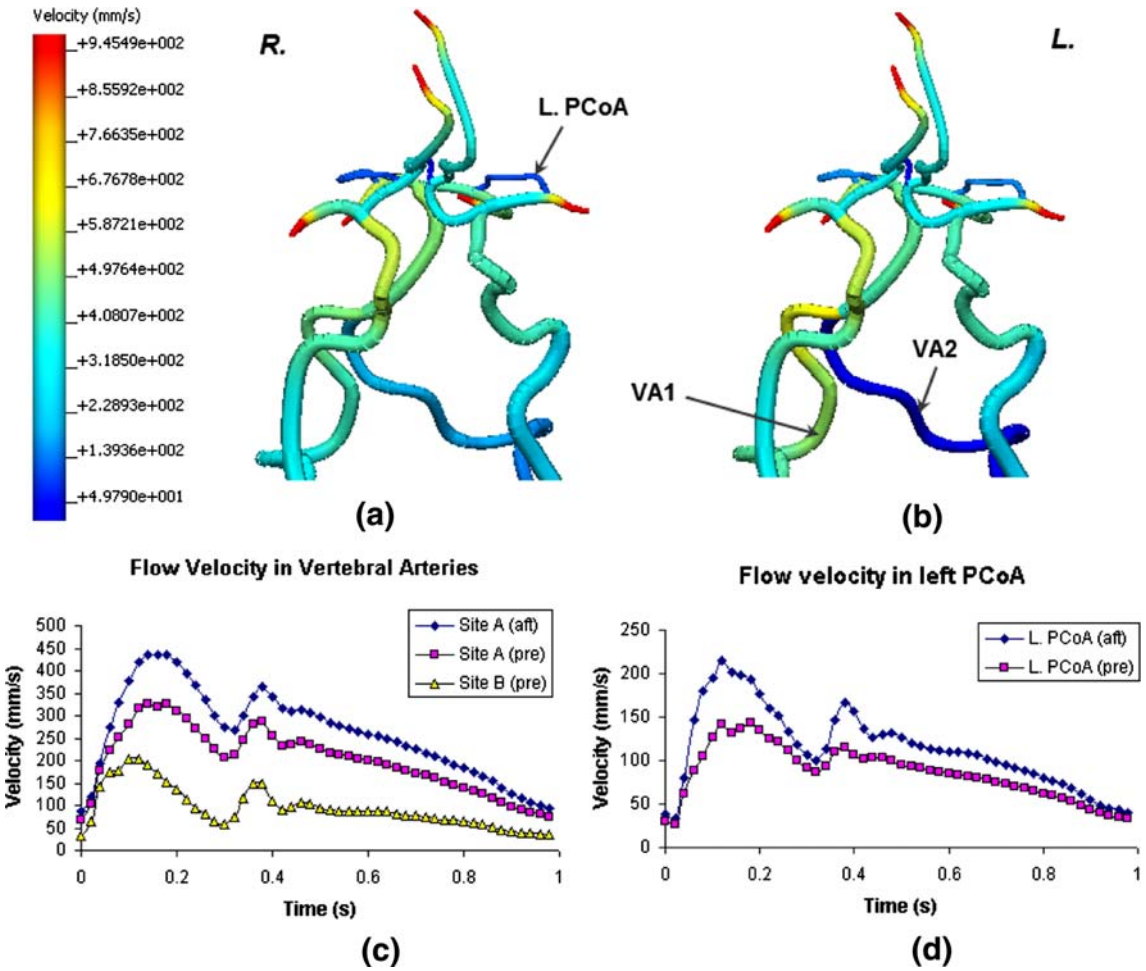

Fig. 8 Effects of vertebral occlusion: **a** velocity distribution in the arterial tree before vertebral occlusion ($t = 0.5$ s); **b** after occlusion (VA2 has no flow; VA1 and L. PCoA have higher velocity); **c** the waveforms of VA1 before and after VA2 occlusion (the average velocity increase in VA1 is about 50 mm/s); **d** flow velocity in L. PCoA has increased by an average of 30 mm/s after VA2 occlusion

a volume CTA image. We simulated the clinical scenario where a vertebral artery was occluded due to severe stenosis or by inflated balloon for cerebral protection. We then observed how flow patterns changed in the vertebral arteries and intracranial arteries. Our simulation suggested that in case of a vertebral artery occlusion, the blood supply to the posterior region of the brain may be compensated from two resources: (1) from the contralateral vertebral artery; (2) from the anterior cerebral arteries. This result agrees qualitatively with the prediction made by a neurosurgeon, who were unaware of our simulation results.

We compared the velocity waveforms of our model with in vivo ultrasonic measurements. The results suggest that the mean flow velocities calculated from our model agree with the ultrasonic data, as well the qualitative shape of the waveform. However, the waveforms computed from our model were flatter than that of ultrasonic measurements in CCA and vertebral arteries. This discrepancy may be improved by using different inflow boundary treatment. We also used a novel out boundary treatment (RSs) to account for the resistance of downstream vessels. A further investigation into its characteristics (length, tapering ratio, elasticity, etc.) associated with different outlets, and a collection of more in vivo data to compare with the computational results, remain as our future work.

It should be mentioned that our model is based on a *generic* arterial tree. This means that the arterial tree has a normal and complete morphology. However, various anatomical formations of the arterial tree exist, which are different from our generic model. For example, about 50% of the population has a CoW with at least one artery absent or hypoplastic [9]. Also, the left vertebral artery may arise directly from the aorta, as occurs in 5% of the population [21]. All of these anatomical variations may lead to hemodynamic patterns different from our simulations. Hence, our computational model should be treated with caution when it comes to clinical significance. On the other hand, with the current computational pipeline, we can quickly modify the generic model to account for the different anatomy and diseases status (e.g. stenosis, occlusion, etc.) therefore make a patient-specific flow model feasible.

Conclusion

As a preliminary study, we have built a computational pipeline to model blood flow in a vertebral angioplasty procedure. We achieved some initial results for the surgical scenario where one of the vertebral arteries is occluded. Our simulation results suggest that the bilateral system together with a complete CoW may still maintain the blood supply in this procedure.

Although this work was designed to model intervention of vertebral arteries, the same techniques can be applied to the hemodynamical study of other vascular diseases, e.g. carotid, aortoiliac and peripheral occlusive diseases.

Acknowledgments We would like to thank Dr. Jian Wu of the Department of Neurosurgery, West China Hospital for sharing his prediction of flow variation in vertebral occlusion procedures. We also thank Dr. Alejandro Frangi of Pompeu Fabra University for providing the CTA image.

References

1. Slovut DP, Bacharach JM (2007) Endovascular therapy for brachiocephalic vessels. In: Rooke TW (ed) chap 27: Vascular medicine and endovascular interventions. Blackwell Futura, Oxford, pp 267–276
2. Rzucidlo EM, Naylor AR (2006) Arch vessel, vertebrovascular, and upper extremity. In: Davies AH, Brophy CM (eds) chap 16, Vascular surgery. Springer, London, pp 181–190
3. Stroud JS, Berger AS, Saloner D (2002) Numerical analysis of flow through a severely stenotic carotid artery bifurcation. J Biomech Eng 124:9–20
4. Perktold K, Resch M, Peter R (1991) Three-dimensional numerical analysis of pulsatile flow and wall shear stress in the carotid artery bifurcation. J Biomech 24:409–420
5. Long Q, Luppi L, Konig CS, Rinaldo V, Das SK (2008) Study of the collateral capacity of the circle of Willis of patients with severe carotid artery stenosis by 3D computational modeling. J Biomech 41:2735–2742
6. Moore SM, Moorhead KT, Chase JG, David T (2005) One-dimensional and three-dimensional models of cerebrovascular flow. J Biomech Eng 127:440–449
7. Smith NP, Pullan AJ, Hunter PJ (2000) An anatomically based model of transit coronary blood flow in the heart. SIAM J App Math 62:990–1018
8. Huo Y, Kassb G (2007) A hybrid one-dimensional/Womersley model of pulsatile blood flow in the entire coronary arterial tree. Am J Physiol Heart Circ Physiol 292:2623–2633
9. Alastruey J, Parker K, Peiro J, Byrd S, Sherwin S (2007) Modelling the circle of Willis to assess the effects of anatomical variations and occlusions on cerebral flows. J Biomech 40:1794–1805
10. Thusitha DSM, Cheng LK, Pullan AJ (2007) A model of blood flow in the mesenteric arterial system. Biomed Eng Online 6:17
11. Zamir M (2005) The physics of coronary blood flow, chap 2. Springer, New York, pp 35–77
12. Chandran KB, Yoganathan AP, Rittgers SE (2006) Biofluid mechanics: the human circulation. CRC Press, Boca Raton
13. Westerhof N, Bosman F, De Vries CJ, Noordergraff A (1969) Analog studies of the human systemic arterial tree. J Biomech 2:121–143
14. Quick CM, Leonard EF, Young WL (2002) Adaptation of cerebral circulation to brain arteriovenous malformations increases feeding artery pressure and decreases regional hypotension. Neurosurgery 50:167–175
15. Formaggia L, Gerbeau JF, Nobile F, Quarteroni A (2001) On the coupling of 3D and 1D Navier–Stokes equations for flow problems in compliant vessels. Comp Meth App Mech Eng 191:561–582
16. Quarteroni A, Tuveri M, Veneziani A (2000) Computational vascular fluid dynamics: problems, models and methods. Comput Visual Sci 2:163–197
17. CMGUI website: http://www.cmiss.org/cmgui

18. Hunter PJ (1972) Numerical solution of arterial blood flow. Master thesis. University of Auckland
19. Anderson JD (1995) Computational fluid dynamics: the basics with applications, chap 6. McGraw-Hill, New York 216–278
20. Fung YC (1996) Biomechanics: circulation, chap 3. Springer, New York
21. Buckenham TM, Wright IA (2004) Ultrasound of the extracranial vertebral artery. Br J Rad 77:15–20
22. Prestigiacomo CJ (2006) Surgical endovascular neuroradiology in the 21st century: what lies ahead?. Neurosurgery 59:48–55